


# A Short Review on Ni-Catalyzed Methanation of CO<sub>2</sub>: Reaction Mechanism, Catalyst Deactivation, Dynamic Operation

Peter Strucks\*, Luisa Failing, and Stefan Kaluza

DOI: 10.1002/cite.202100049

 This is an open access article under the terms of the Creative Commons Attribution License, which permits use, distribution and reproduction in any medium, provided the original work is properly cited.

Today, the use of renewable energies and recycling of climate-changing gases are increasingly important. In this context, coupling of methanation with small, decentralized CO<sub>2</sub> sources such as biogas plants provides one possibility. However, fluctuating availability of renewables for hydrogen production in combination with small storage volumes result in an enhanced demand for dynamic process operation. This leads to new research challenges with respect to the required catalysts and the overall process design. To draw reliable conclusions about the catalytic performance under dynamic process operation, the mechanism of the methanation reaction as well as typical deactivation procedures of the catalyst applied under steady-state conditions have to be reviewed thoroughly.

**Keywords:** CO<sub>2</sub> Methanation, Deactivation, Dynamic operation, Ni catalysts, Power-to-gas

*Received:* April 29, 2021; *revised:* June 11, 2021; *accepted:* July 02, 2021

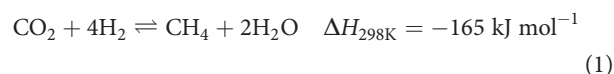
## 1 Introduction

The worldwide consumption of fossil resources related to anthropogenic activities led to an increase of CO<sub>2</sub> emissions in the atmosphere [1]. The debate of the finiteness of fossil fuels and climate change caused research for new technologies over the last years. Methanation of CO<sub>2</sub> with electrolytically produced hydrogen from renewable energies enables chemical energy storage in a cycle (Power-to-Gas) [2] and contributes to the reduction of CO<sub>2</sub> emissions [2–5]. Production of synthetic natural gas (SNG) is of increased interest since it can easily be stored and transported in the already existing gas infrastructure, while being reused for energy generation on demand. However, this technology plays a major role for large CO<sub>2</sub> emitters such as the steel or cement industry [6] but can also be applied at smaller decentralized sites such as biogas plants. In contrast to conventional methane production, CO<sub>2</sub> methanation from biogas raises new challenges regarding fluctuating process conditions and feed gas impurities such as sulfur [7], which may cause deactivation of the most commonly applied nickel catalysts.

Future research activities at the University of Applied Sciences in Düsseldorf will contribute to this topic by investigating the catalytic methanation of CO<sub>2</sub> under dynamic operation conditions. For this purpose, an initial literature survey was conducted focusing on concept concerning reaction mechanism and catalyst deactivation under steady-state conditions as well as on current results on dynamic operation.

## 2 CO<sub>2</sub> Methanation Reaction Mechanism

The catalytic hydrogenation of CO<sub>2</sub> to methane was first reported by Sabatier and Senderens in 1902 [8,9]. It is known that both CO and CO<sub>2</sub> can be reduced over a catalyst in the presence of H<sub>2</sub>, which is shown in Eq. (1) for CO<sub>2</sub> [9,10].



The so-called Sabatier reaction is reversible and exothermic ( $\Delta H_{298\text{K}} = -165 \text{ kJ mol}^{-1}$ ) and is also thermodynamically favorable ( $\Delta G_{298\text{K}} = -130.8 \text{ kJ mol}^{-1}$ ) [11,12]. Additionally, the reaction proceeds with a decrease in volume. This means that, from a thermodynamic point of view, it is favored at low temperature and increased pressure (Le Chatelier's principle). However, the reduction of fully oxidized carbon to methane is a process with significant kinetic limitations and, therefore, requires a catalyst to achieve acceptable rates and selectivities [12,13]. Noble metal or nickel-based catalysts are usually applied in methanation [14–16].

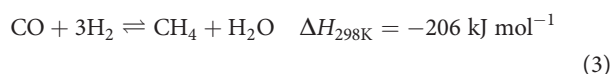
There are various suggestions in literature on how methane is formed. Reaction mechanisms proposed for CO<sub>2</sub> methanation are mainly separated into two groups. The first

Peter Strucks, Luisa Failing, Prof. Dr. Stefan Kaluza  
peter.strucks@hs-duesseldorf.de  
Hochschule Düsseldorf, Fachbereich Maschinenbau und Verfahrenstechnik, Münsterstraße 156, 40476 Düsseldorf, Germany.

mechanism (Fig. 1, paths 1a and b) describes the conversion of CO<sub>2</sub> into the intermediate product CO and subsequent CO methanation. The second mechanism (Fig. 1, path 2) is the direct hydrogenation of CO<sub>2</sub> to methane without initial formation of CO. [17–19]

There is no general agreement on the reaction kinetics and mechanism for methanation of CO<sub>2</sub>, although the first suggestion assuming CO as an intermediate is more popular and, therefore, is described in more detail in the following [20].

The mechanism of CO<sub>2</sub> methanation including intermediate CO is described as a combination of the reverse water-gas shift reaction (RWGS) in Eq. (2) and CO methanation in Eq. (3).

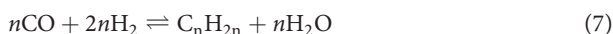
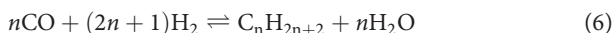


In a first step, CO<sub>2</sub> adsorbs on the catalyst surface, followed by dissociation into CO<sub>ads</sub> and O<sub>ads</sub>. CO<sub>2</sub> methanation afterwards proceeds in the same way as CO methanation [11, 13, 21, 22]: according to reaction path 1a (Fig. 1), adsorbed CO can either dissociate further to form adsorbed carbon and oxygen atoms or desorb from surface. In several intermediate steps, adsorbed carbon is successively hydrogenated to methane, which finally desorbs from the catalyst surface. Simultaneously, adsorbed oxygen is hydrogenated to water. In this mechanism, dissociation of adsorbed CO is regarded as the rate-determining step [21, 23]. Coenen et al. proposed another potentially rate-determining step assuming adsorbed CO first to form an intermediate CHO surface species, according to reaction path 1b, which is successively hydrogenated to methane afterwards [23].

Beside CO formation by the already mentioned RWGS reaction (Eq. (2)), various side reactions can occur leading to decreased methane selectivity [24, 25]. The exothermic Boudouard reaction (Eq. (4)) as well as endothermic methane pyrolysis (Eq. (5)) can lead to the formation of surface carbon:



In addition, hydrocarbons, i.e., alkanes and alkenes can be formed according to Eq. (6) and Eq. (7), respectively (Fischer-Tropsch reaction):



From the thermodynamical point of view, CO<sub>2</sub> methanation should be performed at high pressures and low temperatures. However, for a technical realization, high pressures are of economic disadvantage, while low temperatures strongly reduce the productivity of the process. For this reason, highly active catalysts are necessary and techno-economic compromises still have to be found. [25]

### 3 Nickel-based Methanation Catalysts

Research on methanation of CO<sub>2</sub> focuses on different catalyst systems. Up to now, noble metal catalysts provide the highest performance, with ruthenium considered the most active metal for CO<sub>2</sub> methanation [13, 20]. Rhodium is one of the most investigated metals for CO<sub>2</sub> methanation, while palladium is also described as highly active [20]. However, catalyst systems based on non-noble metals are significantly more cost-effective. A well-known representative of this group is nickel, mostly due to its low costs and high efficiency. Iron as another inexpensive alternative metal is less harmful than Ni [26, 27]. However, in addition to a lower activity, it shows decreased methane selectivity and enhanced CO formation. Nevertheless, recent research suggests that sufficiently dispersed iron may provide an alternative for the commonly used supported Ni catalysts. [28, 29] In addition, bimetallic catalysts are also applied in CO<sub>2</sub> methanation. For instance, Guo and Lu investigated cobalt-nickel catalysts prepared via impregnation on a silica support [30].

In most cases, the solely catalytic active metals are deposited on a support and combined with various promoters to achieve higher activity [31–35]. Metal oxides such as Al<sub>2</sub>O<sub>3</sub>, SiO<sub>2</sub>, CeO<sub>2</sub>, TiO<sub>2</sub>, or ZrO<sub>2</sub> are most commonly used as support. Here, Al<sub>2</sub>O<sub>3</sub> seems to be the most widely studied material, as it provides the ability of high and homogeneous metal dispersion [36–39]. Typical metal or metal oxide

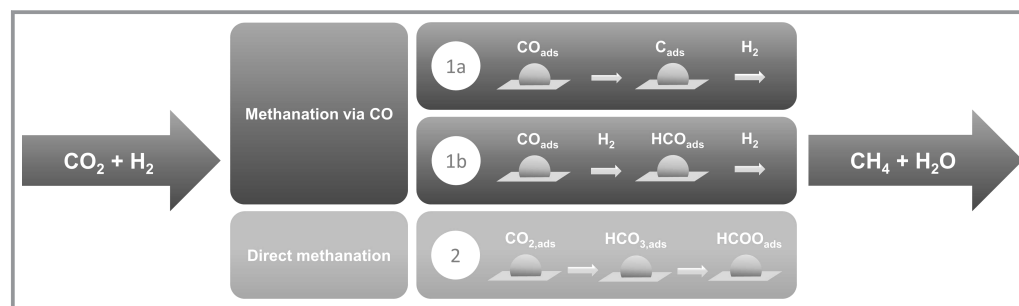


**Figure 1.** Overview of core features of reaction mechanisms for CO<sub>2</sub> methanation.

loadings are reported in the range of 10–40 wt % [30, 36–41].

A selection of currently investigated Ni-based catalyst systems including preparation method, activation procedure, methanation test conditions, and performance results is given in Tab. 1.

### 3.1 Effect of the Support

Ma et al. prepared a series of nickel-based catalysts with four different support materials including characterization and testing in CO<sub>2</sub> methanation at 250–550 °C. Especially at temperatures below 350 °C, they revealed the following order of activity in terms of CO<sub>2</sub> conversion: Ni/CeO<sub>2</sub> > Ni/Al<sub>2</sub>O<sub>3</sub> > Ni/TiO<sub>2</sub> > Ni/ZrO<sub>2</sub>. Mean particle sizes of metallic nickel were approximated from XRD using the Scherrer equation. This resulted in 6.8 nm for Ni/Al<sub>2</sub>O<sub>3</sub>, 8.2 nm for Ni/CeO<sub>2</sub>, 21.9 nm for Ni/TiO<sub>2</sub>, and 33.5 nm for Ni/ZrO<sub>2</sub>. Moreover, the Ni/Al<sub>2</sub>O<sub>3</sub>, Ni/TiO<sub>2</sub>, and Ni/ZrO<sub>2</sub> catalysts showed one single reduction peak, with increasing peak temperatures in the order Ni/ZrO<sub>2</sub> < Ni/TiO<sub>2</sub> < Ni/Al<sub>2</sub>O<sub>3</sub>. This led the authors to the conclusion that highly dispersed nickel particles were almost completely present in the pores

of alumina, resulting in stronger interactions between nickel oxide and the support. In contrast, three reduction peaks were observed for the Ni/CeO<sub>2</sub> catalyst, with the first reduction peak assigned to large NiO particles on the surface of the support and the second peak assigned to the reduction of NiO particles inside the porous structure of the support. The third peak resulted from the reduction of the CeO<sub>2</sub> support. In summary, the H<sub>2</sub>-TPR and TPD results showed that interaction between nickel and the support for the Ni/Al<sub>2</sub>O<sub>3</sub> catalyst was strong and metallic nickel was well dispersed, while more CO<sub>2</sub> was adsorbed at the weak basic sites of the Ni/CeO<sub>2</sub> catalyst. [36]

A series of Ni/ZrO<sub>2</sub> catalysts were synthesized by Li et al. using the urea combustion method. The results indicated that the Ni/ZrO<sub>2</sub>-O catalyst derived from zirconium oxynitrate hydrate has a higher catalytic activity than the Ni/ZrO<sub>2</sub> catalyst. Again, this was attributed to higher Ni dispersion and a lower Ni particle size. Ni/ZrO<sub>2</sub>-O catalyst with a urea-nitrate molar ratio of 0.4 showed the highest catalytic activity due to the highest Ni dispersion, lowest Ni particle size and enhanced metal-support interaction. [41]

Other support materials for nickel-based catalysts are silicon dioxide or silicon carbide. Le et al. prepared Ni/SiC and Ni/SiO<sub>2</sub> catalysts by wet impregnation and deposition-

**Table 1.** Overview of current studies on Ni-based catalyst systems for CO<sub>2</sub> methanation.

Source	Catalyst	Preparation	Activation	<i>T</i> and <i>p</i>	WHSV [mL h <sup>-1</sup> g <sup>-1</sup> ]	Feed	X <sub>CO<sub>2</sub>,max</sub> [%] ( <i>T</i> [°C])	S <sub>CH<sub>4</sub></sub> [%] ( <i>T</i> [°C])
[36] 2020	20Ni/CeO <sub>2</sub>	deposition precipitation	4 h, 600 °C, 10 % H <sub>2</sub> in N <sub>2</sub> , 50 mL min <sup>-1</sup>	250–550 °C, 1 bar	120 000	H <sub>2</sub> /CO <sub>2</sub> /N <sub>2</sub> 4:1:1	~70 (400)	~97 (400)
	20Ni/Al <sub>2</sub> O <sub>3</sub>						~69 (400)	~94 (400)
	20Ni/TiO <sub>2</sub>						~67 (400)	~94 (400)
	20Ni/ZrO <sub>2</sub>						~62 (550)	~69 (550)
[41] 2018	15Ni/ZrO <sub>2</sub> -O	urea combustion	2 h, 500 °C, 50 % H <sub>2</sub> in N <sub>2</sub> , 60 mL min <sup>-1</sup>	250–500 °C, 1 bar	50 000	H <sub>2</sub> /CO <sub>2</sub> /N <sub>2</sub> 36:9:5	~82 (400)	~99 (400)
	15Ni/ZrO <sub>2</sub>						~76 (400)	~98 (400)
[40] 2018	10–20Ni/SiO <sub>2</sub>	wet impregna- tion	1 h, 500 °C, 100 % H <sub>2</sub>	150–400 °C, 1 bar	60 000	H <sub>2</sub> /CO <sub>2</sub> /He 50:1:49	~100 (400)	–
	10–20Ni/SiC	deposition					~100 (400)	–
[37] 2019	20–40Ni/Al <sub>2</sub> O <sub>3</sub>	impregnation	2 h, 600 °C, 100 % H <sub>2</sub>	200–600 °C, 1.9 bar	30 000	H <sub>2</sub> /CO <sub>2</sub> /Ar 62:15:23	~91 (350)	~100 (350)
	20–40Ni-5Ce/ Al <sub>2</sub> O <sub>3</sub>						~93 (325)	~100 (325)
[38] 2015	Ni/Al <sub>2</sub> O <sub>3</sub>	incipient wet impregnation method	2 h, 400 °C, 64 % H <sub>2</sub> in N <sub>2</sub> , 70 mL min <sup>-1</sup>	380–500 °C, 1 bar	30 000	H <sub>2</sub> /CO <sub>2</sub> /N <sub>2</sub> 36:9:5	~84 (450)	~100 (450)
	Ni-2Ce/Al <sub>2</sub> O <sub>3</sub>						~87 (400)	~100 (400)
	Ni/2Ce-Al <sub>2</sub> O <sub>3</sub>						~84 (450)	~100 (450)
[39] 2016	15Ni/Al <sub>2</sub> O <sub>3</sub>	incipient wet impregnation method	2 h, 500 °C, 50 % H <sub>2</sub> in N <sub>2</sub> , 60 mL min <sup>-1</sup>	250–500 °C, 1 bar	48 000	H <sub>2</sub> /CO <sub>2</sub> /N <sub>2</sub> 36:9:5	~83 (450)	~99 (450)
	15Ni-Mn/Al <sub>2</sub> O <sub>3</sub>						~85 (400)	~99 (400)
[30] 2014	Co <sub>x</sub> -Ni/SiO <sub>2</sub>	wet co-impregna- tion	3 h, 450 °C, 50 % H <sub>2</sub> in N <sub>2</sub> , 60 mL min <sup>-1</sup>	250–450 °C, 1 bar	13 200	H <sub>2</sub> /CO <sub>2</sub> /N <sub>2</sub> 8:2:1, 6:2:3, 4:2:5	~78 (400) ~83 (350)	~93–99

precipitation for CO and CO<sub>2</sub> methanation. H<sub>2</sub>-TPR results showed that precipitated catalysts exhibited stronger interaction between nickel oxide and the support compared to the catalysts prepared via wet impregnation. Precipitated Ni/SiC catalyst also showed a higher activity than an impregnated Ni/SiC catalyst. High Ni dispersion obtained by precipitation in combination with high thermal conductivity provided by SiC are assumed to be beneficial for both CO and CO<sub>2</sub> methanation. Furthermore, the activity of impregnated Ni/SiC and Ni/SiO<sub>2</sub> catalysts increased with an increased nickel content. [40]

### 3.2 Effect of Promoters

Commonly reported promoters for Ni-catalyzed methanation are CeO<sub>2</sub> or MnO<sub>2</sub>. For instance, Gac et al. [37] and Li et al. [38] showed that the catalytic activity at low reaction temperatures of a Ni/Al<sub>2</sub>O<sub>3</sub> catalyst was improved by addition of a ceria promoter together with higher nickel loadings. Moreover, the catalysts showed high resistance towards sintering and carbon deposition at high reaction temperatures [37]. Addition of 2 wt % of CeO<sub>2</sub> either to the active metal or the catalyst support favored CO<sub>2</sub> methanation. When CeO<sub>2</sub> was added to nickel, dispersion of the nickel particles was increased, and the nickel particle size decreased. This resulted in a stronger interaction between nickel and Al<sub>2</sub>O<sub>3</sub>, which was related to the shift of the measured TPR profiles towards higher peak temperatures. In addition, CO<sub>2</sub> conversion was increased. When CeO<sub>2</sub> was added to Al<sub>2</sub>O<sub>3</sub>, CO<sub>2</sub> conversion also increased, but the effect was lower compared to the direct addition of CeO<sub>2</sub> to nickel. [38]

Zhao et al. impregnated a Ni/Al<sub>2</sub>O<sub>3</sub> catalyst with manganese as a promoter. Addition of manganese increased the number of CO<sub>2</sub> adsorption sites and inhibited the agglomeration of Ni particles due to improved Ni dispersion and weaker interactions between the nickel species and the support. The manganese content was varied between 0.86 and 2.54 %, with the highest CO<sub>2</sub> conversion achieved for a Mn-Ni/Al<sub>2</sub>O<sub>3</sub> catalyst containing 1.71 % manganese. The catalytic activity was increased especially at low temperatures. [39] Studies by Abate et al. on Ni-based mixed oxide supported catalysts provided similar results. They studied Ni/Al<sub>2</sub>O<sub>3</sub> catalysts with varying loadings of ZrO<sub>2</sub>, TiO<sub>2</sub>, and CeO<sub>2</sub> and obtained increasing conversion rates with increased loading at 300 °C. The higher performance of Ni-based mixed oxide supported catalysts was explained by the improved reducibility as determined by H<sub>2</sub>-TPR. [42]

## 4 Deactivation

The prevention of catalyst deactivation leads to challenges with respect to construction and operation of large-scale catalytic processes, but also in coupling the technology with

smaller, decentralized sources such as biogas plants. In literature, deactivation of nickel-based methanation catalysts is mainly attributed to sintering, poisoning, and carbon deposition.

### 4.1 Sintering

Thermal sintering caused by high reaction temperatures or exothermal hot spot formation is probably the main reason for decreasing nickel surface area during methanation [43]. In principle, thermal sintering is attributed to surface diffusion or, if temperatures are high enough, mobility of larger aggregates [44].

In this context, the so-called Tamman and Hüttig temperatures are considered, which are directly related to the melting temperature of the respective metal species. For nickel, the melting temperature is 1726 K [45]. The mobility of atoms increases with increasing temperature. When the Hüttig temperature is reached, the mobility of the atoms first occurs at defect sites [44, 46]:

$$T_{\text{Hüttig}} = 0.3T_{\text{melt}} \quad (8)$$

For nickel, this results in  $T_{\text{Hüttig}} = 518$  K. With further increase in temperature, bulk atom mobility occurs when the Tamman temperature is reached:

$$T_{\text{Tamman}} = 0.5T_{\text{melt}} \quad (9)$$

For nickel, this results in  $T_{\text{Tamman}} = 863$  K. Reaching the melting temperature finally leads to liquid phase behavior of the metal. Although these temperatures are above the usually applied methanation reaction temperature, local temperatures inside the catalyst bed (hot spots) can significantly exceed this value due to the highly exothermic reaction.

Support materials can also suffer from sintering at high temperatures. Therefore, materials exhibiting high thermal stability and high melting points are commonly chosen as catalyst support, e.g., Al<sub>2</sub>O<sub>3</sub> with a melting point of 2323 K [47]. For CeO<sub>2</sub>, the melting temperature is 2273 K [48] and for TiO<sub>2</sub> it is 2128 K [49].

Rostrup-Nielsen et al. investigated sintering during methanation of synthesis gas for more than 8000 h time on stream (TOS). As a mathematical approach describing the loss of active surface, they derived a power law regarding the relative nickel particle diameter as a function of TOS [50]:

$$\frac{d_{\text{Ni}}(t)}{d_{\text{Ni}}^0} = (1 + k_{\text{sint}}t)^n \quad (10)$$

where  $d_{\text{Ni}}(t)$  is the nickel crystal size after a certain TOS ( $t$ ),  $d_{\text{Ni}}^0$  is the nickel crystal size before sintering,  $k_{\text{sint}}$  is the sintering rate constant, and  $n$  is the sintering order. Fuentes and Bartholomew quantitatively described decreasing dis-

persion during reaction using a general power law expression (GPLe) [51, 52]:

$$-\frac{d(D/D_0)}{dt} = k'_{\text{sint}} \left( \frac{D}{D_0} - \frac{D_{\text{eq}}}{D_0} \right)^{n'} \quad (11)$$

where  $D_0$  is the initial dispersion,  $D$  is the actual dispersion,  $k'_{\text{sint}}$  is the sintering rate constant,  $n'$  is the order of sintering, that is found to be either 1 or 2. The term  $-D_{\text{eq}}/D_0$  takes into account the asymptotic approach of a typical dispersion-time curve for a limit dispersion  $D_{\text{eq}}$  at infinite time. [52]

In this context, further publications investigated and described in particular Ni-based methanation catalysts [53] and the exposed metallic surface as a function of time [54] as well as the influence of  $\text{H}_2\text{O}/\text{H}_2$  ratio [55, 56].

Champon et al. performed measurements of  $\text{CO}_2$  methanation catalyst activity by fresh and post-mortem catalysts that had previously been aged under hydrothermal conditions for various times. A change of the nickel particle size distribution for the aged samples was determined by transmission electron microscopy (TEM) images (Fig. 2). For TEM images, the average metal particle size was obtained from several measurements in two orthogonal directions. A sample of 30 particles found a growth in average metal particle size from 6.5 nm for a sample aged for 20 h up to 10.5 nm for a sample aged for 100 h. [57]

$\text{CO}_2$  conversions and  $\text{CH}_4$  yields of catalysts after hydrothermal aging of different periods are shown in Fig. 3. Both parameters significantly decrease with increasing aging time.

The loss of activity was assumed to correlate to the observed decrease of the metallic surface. This confirms the general opinion that sintering of nickel particles is a major cause of deactivation for methanation catalysts. [57]

Champon et al. determined the loss of metal surface due to sintering of metal particles by measuring metal surfaces with hydrogen chemisorption and temperature-programmed desorption ( $\text{H}_2$ -TPD). They adapted the GPLe previously proposed by Fuentes [51] taking into account that higher  $\text{H}_2\text{O}/\text{H}_2$  ratios promote sintering [57]:

$$-\frac{d(S(t)/S_0)}{dt} = k_{\text{sint,ref}} \exp\left(-\frac{E_{\text{A,sint}}}{R} \left(\frac{1}{T_{\text{ref}}} - \frac{1}{T}\right)\right) \left(\frac{S(t)}{S_0} - \frac{S_{\text{eq}}}{S_0}\right)^2 \left(\frac{p_{\text{H}_2\text{O}}}{p_{\text{H}_2}}\right)^q \quad (12)$$

The approach includes the kinetic sintering constant at a reference temperature of  $600^\circ\text{C}$  ( $k_{\text{sint,ref}}$ ), the sintering acti-

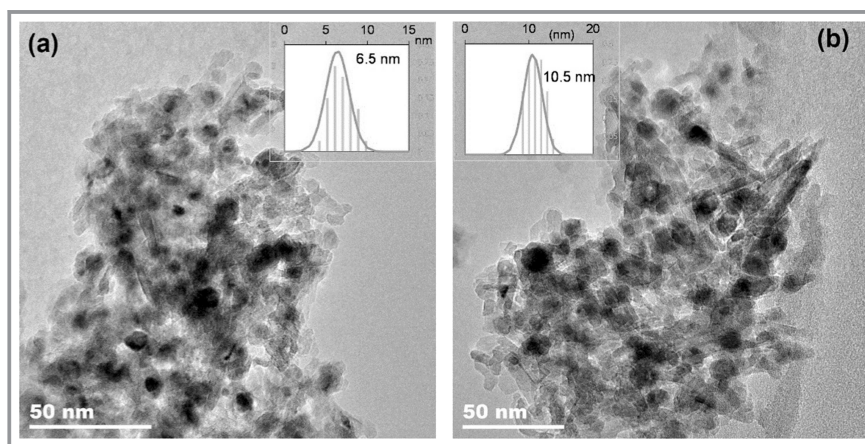


**Figure 2.** TEM images and nickel particle size distribution for catalyst samples aged for a) 20 h and b) 100 h under hydrothermal conditions ( $600^\circ\text{C}$ , ratio of  $\text{H}_2\text{O}$  to  $\text{H}_2 = 0.26$ ) [57].

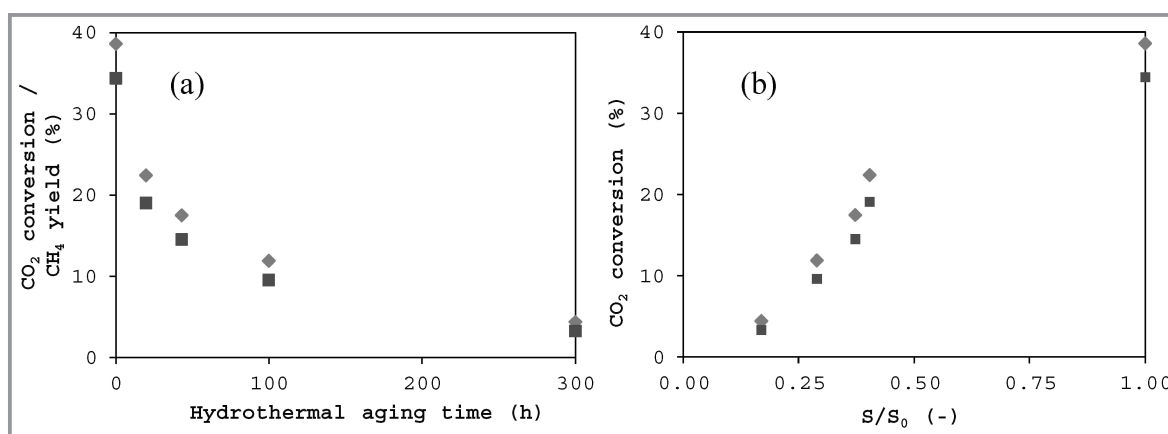


**Figure 3.** Measurements of  $\text{CO}_2$  conversion and  $\text{CH}_4$  yield at  $350^\circ\text{C}$  of fresh and post-mortem samples, which were previously hydrothermally aged, as a function of a) the hydrothermal aging time and b) the relative metallic surface.

◆,  $\text{CO}_2$  conversion; ■,  $\text{CH}_4$  yield. [57]

vation energy ( $E_{A,sint}$ ), the metallic equilibrium surface, i.e., the metallic surface that was obtained at infinite sintering time ( $S_{eq}$ ), and the exponent  $q$ . After numerically integrating, the four parameters for an initial area of  $10\text{ m}^2\text{g}^{-1}$  and a reference temperature of  $600\text{ }^\circ\text{C}$  were revealed by the method of least squares minimization:  $k_{sint,ref} = 0.32\text{ h}^{-1}$ ,  $E_{A,sint} = 126\text{ kJ mol}^{-1}$ ,  $S_{eq}/S = 0.19$ , and  $q = 0.63$ . Taking temperature and local atmosphere into account, the GPLC was able to describe the nickel particle sintering depending on TOS (for up to 300 h) for a Ni/Al<sub>2</sub>O<sub>3</sub> catalyst at temperatures between 450 and 600 °C and H<sub>2</sub>O/H<sub>2</sub> ratios between 0 and 3.2 with an error of  $\pm 15\%$ . [57] In future studies, the group will further investigate the catalytic activity depending on the operating time under the reactive conditions of CO<sub>2</sub> methanation (H<sub>2</sub>/CO<sub>2</sub> = 4). The aim is to relate experimental deactivation results with modeled ones by coupling a kinetic model of CO<sub>2</sub> methanation [58] with the previously shown sintering law.

Beside the active phase, sintering can also affect the support. For instance, additives or impurities can occupy defects in or form new phases with the support. In particular with respect to the Ni/Al<sub>2</sub>O<sub>3</sub> system, a thermally stable NiAl<sub>2</sub>O<sub>4</sub> spinel phase is formed at higher temperatures, decreasing the reducibility of nickel oxide [59]. In addition to sintering of the catalytic active material, steam also accelerates sintering of the support by forming hydroxyl groups on the surface, which can be volatilized at high temperatures. Moreover, dispersed metals inside the support can cause enhanced sintering. In case of Ni/Al<sub>2</sub>O<sub>3</sub> catalysts applied in methanation, dispersed nickel accelerates the loss of Al<sub>2</sub>O<sub>3</sub> surface. [52, 59, 60] For those reasons, recent studies investigate the influence of various promoters to reduce sintering of both the catalytic active phase and the support materials [31, 61–64].

Catalytic testing is usually performed under isothermal conditions. However, due to the exothermic nature of the reaction, hot spots inside the catalyst bed can form, which strongly promote sintering. Türks et al. investigated the formation of hot spots as a function of the amount of catalyst used together with the reactor design. An increasing catalyst amount led to an increased productivity but was accompanied by a simultaneous increase of the hot spot temperatures. However, this hot spot formation was significantly reduced by applying a reactor with several separate and variably diluted fixed beds. [65] Pérez et al. also investigated an alternative reactor concept for CO<sub>2</sub> methanation. Experiments were carried out in a multichannel microreactor system at 15 bar and temperatures between 200 and 400 °C. Due to improved heat removal compared to a simple fixed bed reactor, hot spot formation was suppressed even at high conversions. [66]

## 4.2 Poisoning

Ni-catalyzed hydrogenation reactions are generally sensitive to poisoning by compounds containing S, P, As, Zn, Hg, halides, Pb, NH<sub>3</sub>, and C<sub>2</sub>H<sub>2</sub> [52]. However, poisoning studies mainly focus on sulfur components, i.e., especially H<sub>2</sub>S, as these usually represent severe contaminations in methanation feedstocks [67, 68]. In general, H<sub>2</sub>S shows a higher toxicity than compounds with oxidized sulfur, such as SO<sub>2</sub> [59]. Deactivation of Ni-based catalysts due to poisoning by H<sub>2</sub>S strongly depends on its concentration or partial pressure [69].

Rostrup-Nielsen et al. described a strong nonlinear decrease in activity due to blocking of active sites with the following approach [50]:

$$\frac{r_S}{r_0} = (1 - \theta_S)^m \quad (13)$$

where  $r_S$  is the methanation rate of S-poisoned catalyst,  $r_0$  is the methanation rate of non-poisoned catalyst,  $\theta_S$  is the sulfur coverage of nickel surface, and  $m$  is the number of atoms that form an active site for methanation. The group explained the strong nonlinear dependence of the methanation rate on the sulfur coverage by assuming an ensemble of 10 Ni atoms being involved in CO<sub>2</sub> methanation. This results in  $m = 10$  in the equation shown above.

As already described, Ni-catalyzed methanation is a structure-sensitive reaction with an activity and selectivity highly depending on the metal dispersity [50, 70, 71]. Thus, a change in surface geometry is particularly crucial in this case [44, 52].

Gac et al. performed poisoning studies on impregnated Ni/Al<sub>2</sub>O<sub>3</sub> catalysts with high nickel dispersion. The data obtained indicated that high loadings as well as the use of Ce as a promoter led to an increase in active surface. All catalysts showed high initial activity for CO<sub>2</sub> methanation performed at 475 °C. [37]

Constant conversion and high CH<sub>4</sub> selectivity were observed during the first 20 h TOS (Fig. 4). Then, H<sub>2</sub>S was added to the feed gas with an overall concentration of 8 ppm. After additional 20 h TOS, deactivation was observed by a strong decrease of CO<sub>2</sub> conversion. Deactivation was attributed to a continuous sulfur poisoning of the exposed Ni particles successively affecting the complete catalyst bed. Conversion then stagnated at a low level with CH<sub>4</sub> selectivity decreasing at the same time resulting in CO being the major reaction product (RWGS). The investigations showed that the operating time of the catalysts can be extended by increasing the metal loading and by adding Ce as a promoter, both resulting in higher metal dispersion. In situ DRIFTS studies of fresh and spent catalysts indicated that deactivation of the catalysts is attributed to the hindering of the initial step of CO<sub>2</sub> methanation reaction, i.e., formation of surface carbonyl species and subsequent hydrogenation to methane. In addition, it was found that the

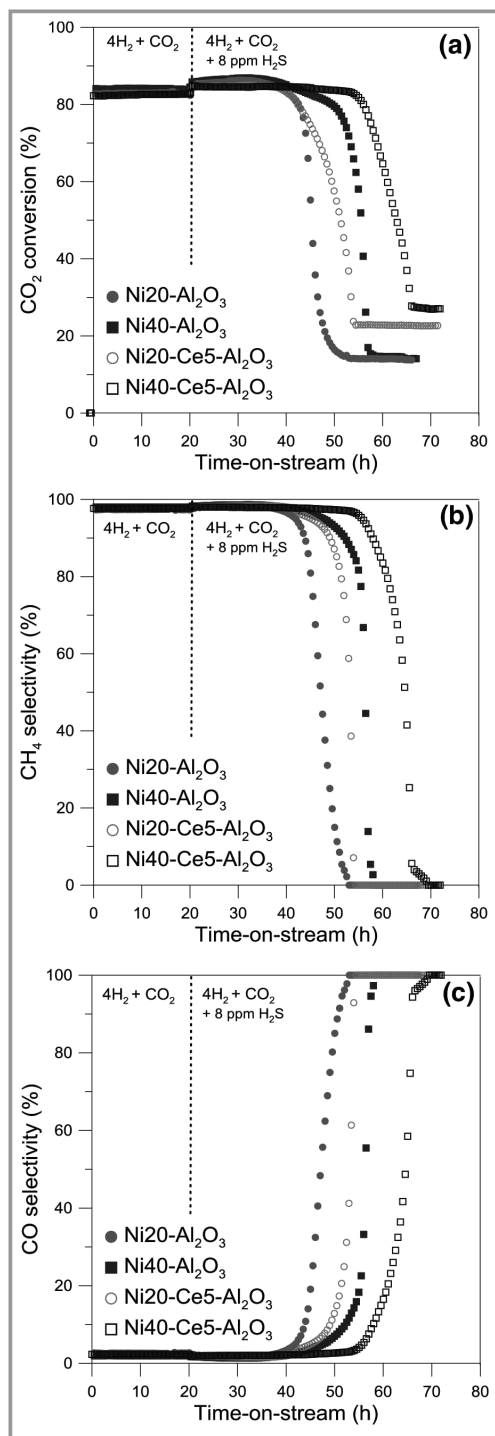


**Figure 4.** Performance of nickel-based catalysts under methanation conditions and after introduction of 8 ppm H<sub>2</sub>S. a) CO<sub>2</sub> conversion, b) CH<sub>4</sub> selectivity, c) CO selectivity. [37]

presence of the Ce promoter might change the deactivation process of the catalyst, since conversion of CO<sub>2</sub> molecules to suitable intermediate species is facilitated. Sulfur adsorption is an exothermic process and, therefore, temperature-dependent. However, at moderate reaction temperatures, as

mostly present in methanation, sulfur poisoning can be considered irreversible. [37, 72, 73]

Méndez-Mateos et al. also investigated the deactivation of Ni/Al<sub>2</sub>O<sub>3</sub> catalysts caused by H<sub>2</sub>S. In addition, influences of Co, Cr, Fe, and Mo as promoters were investigated. While higher amounts of Mo (8 wt %) led to blocking of the active Ni sites and, thus, to reduced activity, small amounts (4 wt %) improved the methanation reaction. [74] Bartholomew explained this effect with the fact that Mo can selectively adsorb sulfur and, thereby, increase sulfur resistance of Ni catalysts [52].

### 4.3 Carbon Deposition

Various studies report carbon deposition during CO methanation, which is prevented by favorable CO/H<sub>2</sub> ratios as well as the presence of steam [75–79]. CO<sub>2</sub> methanation, as already discussed, is the combination of the RWGS reaction followed by CO methanation. This leads to a significant amount of steam being permanently present in the reaction atmosphere and might explain why significant carbon deposition does not occur in CO<sub>2</sub> methanation experiments: under stoichiometric conditions and at elevated pressures, no obvious deactivation due to carbon deposition was observed in various studies considering the stability of nickel-based catalysts for methanation [37, 42, 78, 80–83].

Nevertheless, with regard to investigations of the deactivation behavior under dynamic process conditions and, therefore, associated fluctuations in the feed gas composition, possible deactivation by carbon deposition should still be taken into account.

## 5 CO<sub>2</sub> Methanation under Dynamic Conditions

Dynamic operation of methanation reactors is preferred to reduce the upstream storage capacity but is not fully understood in current literature [84]. Recently, only few publications were found dealing with investigations of the deactivation behavior of Ni-based catalysts in the context of dynamic operation. In the investigations reported, repetitive interruption of the H<sub>2</sub> feed imitating fluctuating H<sub>2</sub> streams resulting from renewable energies was performed.

Kreitz et al. investigated dynamic methanation of CO<sub>2</sub> on impregnated Ni/Al<sub>2</sub>O<sub>3</sub> catalysts with 10 wt % nickel loading. Steady-state and dynamic studies were performed at a moderate temperature of 300 °C and a pressure of 2 bar. A catalyst mass of 0.5 g and a flow rate of 400 mL<sub>N</sub>min<sup>-1</sup> were used, resulting in a gas hourly space velocity (GHSV) of 46 375 h<sup>-1</sup>. The reactor was alternately fed with a H<sub>2</sub>/Ar mixture and a CO<sub>2</sub>/He mixture, respectively. Different cycle times and cycle split ratios were applied. Fig. 5 shows an exemplary cycle with a duration of 60 s and a cycle split ratio of 0.5. The numerical values in parentheses are the

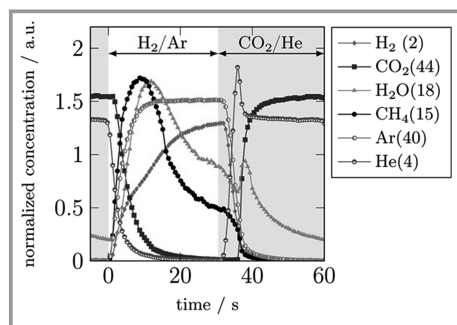


**Figure 5.** Normalized ion current profiles of an exemplary cycle of 60 s with a cycle split ratio of 0.5. Reproduced from [85] with permission from Wiley.

mass-to-charge ratios on which the components are measured with a quadrupole mass spectrometer. Individual normalization was performed for each signal, therefore, the amplitudes of the signal cannot be compared and the figure is only a qualitative visualization. During the  $\text{H}_2/\text{Ar}$  cycle, a high methane formation rate was observed, which immediately decreased during the  $\text{CO}_2/\text{He}$  cycle.

This behavior is due to the fact that  $\text{CO}_2$  is first adsorbed on the surface of the catalyst during the  $\text{CO}_2/\text{He}$  cycle, which is subsequently hydrogenated during the  $\text{H}_2/\text{Ar}$  cycle. Since the catalyst can only adsorb a certain amount of  $\text{CO}_2$  on the active sites, methanation stagnates during the  $\text{H}_2/\text{Ar}$  cycle. Since the adsorption of  $\text{CO}_2$  proceeds at a high rate, the surface can be saturated even at small cycle split ratios. Reduced cycle time and a stoichiometric cycle split rate will increase the average reaction rate by shortening the period without methanation. No improvement in steady-state results was achieved. There is a constant activity of the catalyst used over the entire experimental duration (corresponds to max. 100 min), which showed that no significant deactivation of the Ni catalyst occurred even under these conditions. [85]

Mutz et al. also investigated  $\text{Ni}/\text{Al}_2\text{O}_3$  catalysts with a nickel loading of 10 wt % under dynamic methanation conditions with a total duration of about 500 min after activation. The catalysts were alternately loaded with reactants in the ratio  $\text{H}_2/\text{CO}_2 = 4$  and a less reducing atmosphere by absence of  $\text{H}_2$  and investigated by operando X-ray absorption spectroscopy (XAS). In absence of  $\text{H}_2$ , rapid phase transformations between metallic nickel,  $\text{NiO}$ , and  $\text{NiCO}_3$  occurred, which can be attributed to an oxidation of active sites. After returning to initial methanation conditions, Ni particles were shown to be only partially recovered. Complete regeneration was only possible by reactivation in hydrogen at high temperatures. Overall, a slight but continuous deactivation of the catalyst was evident during the investigations. [86]

In further investigations, it was shown that the frequency of  $\text{H}_2$  interruption also has an influence on the catalytic performance and, especially, on the deactivation. A longer interruption of the  $\text{H}_2$  feed resulted in a stronger deactivation due to bulk oxidation. [87]

Recent studies focused on modeling and simulation of dynamic methanation. Theurich et al. studied the dynamic operation of a fixed-bed recycle reactor with flow ramps and varied ramp times. During transition, the highest methane contents were achieved when the flow rate was reduced and the highest gas temperature when the flow rate was increased. In addition, the influence of recirculation was investigated, which might be a possibility to stabilize the reactor behavior under fluctuating conditions. [84] Bremer et al. investigated the optimization of the reactor startup to avoid hot spot formation [88]. Fache et al. modeled the intermittent operation of a fixed-bed methanation reactor and its ability to restart after a shutdown. Furthermore, the possibility of the reactor being able to restart due to its own thermal inertia and exothermicity of the reaction without requiring external heating was examined. [89] Simulations by Rönsch et al. primarily identified a high temperature occurrence in dynamic operation of methanation reactors as a critical effect [90, 91]. Kinetic modeling and simulation of methanation reactors has been reviewed in detail by Rönsch et al. [92].

## 6 Conclusion

Coupling methanation with small, decentralized  $\text{CO}_2$  sources such as biogas plants will only be feasible if the process is suitable from a techno-economic point of view and the catalysts used are highly active, inexpensive, and stable over the long term. Due to high activity at low cost, nickel still is in the focus of current research dealing with  $\text{CO}_2$  methanation.

Several possible reaction mechanisms for  $\text{CO}_2$  methanation are discussed in literature, with many publications assuming that the RWGS reaction occurs first, followed by CO methanation. Deactivation mechanisms have already been reviewed in detail [44, 52, 60, 93] and occur for  $\text{CO}_2$  methanation from biogas on Ni-based catalysts mainly due to high temperatures (sintering) or impurities, especially sulfur compounds, in feed gases (poisoning).

Previous knowledge of deactivation was mostly determined under steady-state conditions. Coupling methanation to small, decentralized  $\text{CO}_2$  sources and the electrolysis of hydrogen from renewable energy leads to new challenges. The resulting need for dynamic operation due to fluctuating gas flows, is increasingly the subject of current research. In this context, it is important to reveal which kinds of dynamics might have an impact on the long-term performance of the catalysts used – such as fluctuations in the feed gas streams occurring just for a few seconds up to several hours, system downtimes and restarts, hot spot formation due to fluctuating gas composition – and how distinct possible effects are. This is the initial point for future research activities at the University of Applied Sciences in Düsseldorf.



Open access funding enabled and organized by Projekt DEAL.



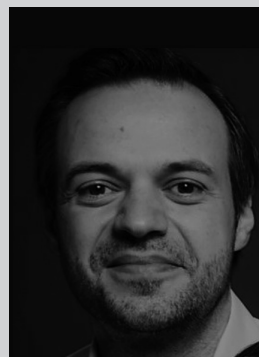
**Peter Strucks** studied Process, Energy and Environmental Technology at Hochschule Düsseldorf – University of Applied Sciences and obtained his Bachelor of Engineering in 2014. Afterwards he studied Simulation and Experimental Engineering and concluded his Master of Science in 2019. Since 2014, he is a research assistant at

Hochschule Düsseldorf and supports education and research in the field of process engineering. Since November 2020, he is doing his doctorate in cooperation with Prof. Doetsch (Ruhr-University of Bochum) in the field of catalytic methanation of CO<sub>2</sub> under dynamic process conditions.



**Luisa Failing** studied Environmental and Process Technology at Hochschule Düsseldorf – University of Applied Sciences and obtained her Bachelor of Engineering in April 2021. She is currently studying for a master's degree in Simulation and Experimental Engineering and supports the group of Prof. Kaluza as a student

assistant in education and research. The focus of her activities is on heterogeneous catalysis, especially in the field of catalytic methanation of CO<sub>2</sub>.



**Stefan Kaluza** studied Chemistry at University of Cologne, where he graduated in 2006. Then, he joined the Muhler group at Ruhr-University of Bochum, working in the field of methanol synthesis and receiving his Ph.D. in 2009. In 2012, he moved on to Fraunhofer Institute for Environmental, Safety, and

Energy Technology UMSICHT in Oberhausen, where he established a research group on heterogeneous catalysis. Since 2018, he is Professor of Industrial Chemistry and Catalysis at the Faculty of Mechanical and Process Engineering, Hochschule Düsseldorf – University of Applied Sciences. The current focus of his research is on catalysis and reaction engineering in the field of CO<sub>2</sub> utilization.

### Symbols used

$D$	[-]	actual dispersion
$D_0$	[-]	initial dispersion
$D_{eq}$	[-]	limit dispersion
$d_{Ni}^0$	[nm]	initial nickel crystal size
$d_{Ni}(t)$	[nm]	nickel crystal size after a certain TOS
$E_{A,sint}$	[kJ mol <sup>-1</sup> ]	sintering activation energy
$GHSV$	[h <sup>-1</sup> ]	gas hourly space velocity
$\Delta G_{298K}$	[kJ mol <sup>-1</sup> ]	standard free energy of reaction
$\Delta H_{298K}$	[kJ mol <sup>-1</sup> ]	standard enthalpy of reaction
$k_{sint}$	[h <sup>-1</sup> ]	sintering constant
$m$	[-]	number of atoms forming an active site
$n$	[-]	sintering order
$r_0$	[mol kg <sup>-1</sup> s <sup>-1</sup> ]	methanation rate of non-poisoned catalyst
$r_S$	[mol kg <sup>-1</sup> s <sup>-1</sup> ]	methanation rate of S-poisoned catalyst
$S(t)$	[m <sup>2</sup> g <sup>-1</sup> ]	metallic surface after a certain TOS
$S_0$	[m <sup>2</sup> g <sup>-1</sup> ]	initial metallic surface
$S_{CH_4}$	[%]	methane selectivity
$S_{eq}$	[m <sup>2</sup> g <sup>-1</sup> ]	metallic surface at infinite sintering time
$t$	[s, min, h]	time (on stream)
$T$	[K, °C]	temperature
$WHSV$	[mL h <sup>-1</sup> g <sup>-1</sup> ]	weight hourly space velocity
$X_{CO_2}$	[%]	CO <sub>2</sub> conversion
$\theta_S$	[-]	sulfur coverage of Ni-surface

## Abbreviations

a.u.	arbitrary unit
DRIFTS	diffuse reflectance infrared Fourier transform spectroscopy
GPLe	general power law expression
H <sub>2</sub> -TPD	temperature programmed desorption after H <sub>2</sub> -chemisorption
H <sub>2</sub> -TPR	temperature programmed reduction with H <sub>2</sub>
RWGS	reverse water gas shift
SNG	synthetic natural gas
TEM	transmission electron microscopy
TOS	time on stream
XRD	X-ray diffraction

## References

- [1] S. N. Riduan, Y. Zhang, *Dalton Trans.* **2010**, 39 (14), 3347–3357. DOI: <https://doi.org/10.1039/b920163g>
- [2] M. Götz, J. Lefebvre, F. Mörs, A. McDaniel Koch, F. Graf, S. Bajohr, R. Reimert, T. Kolb, *Renewable Energy* **2016**, 85, 1371–1390. DOI: <https://doi.org/10.1016/j.renene.2015.07.066>
- [3] K. Hashimoto, M. Yamasaki, K. Fujimura, T. Matsui, K. Izumiya, M. Komori, A. El-Moneim, E. Akiyama, H. Habazaki, N. Kumagai, A. Kawashima, K. Asami, *Mater. Sci. Eng., A* **1999**, 267 (2), 200–206. DOI: [https://doi.org/10.1016/S0921-5093\(99\)00092-1](https://doi.org/10.1016/S0921-5093(99)00092-1)
- [4] J. Lefebvre, M. Götz, S. Bajohr, R. Reimert, T. Kolb, *Fuel Process. Technol.* **2015**, 132, 83–90. DOI: <https://doi.org/10.1016/j.fuproc.2014.10.040>
- [5] T. Trost, S. Horn, M. Jentsch, M. Sterner, *Z. Energiewirtschaft.* **2012**, 36 (3), 173–190. DOI: <https://doi.org/10.1007/s12398-012-0080-6>
- [6] M. A. A. Aziz, A. A. Jalil, S. Triwahyono, A. Ahmad, *Green Chem.* **2015**, 17 (5), 2647–2663. DOI: <https://doi.org/10.1039/C5GC00119F>
- [7] S. Schiebahn, T. Grube, M. Robinus, L. Zhao, A. Otto, B. Kumar, M. Weber, D. Stolten, in *Transition to Renewable Energy Systems* (Eds: D. Stolten, V. Scherer), Wiley-VCH, Weinheim **2013**.
- [8] P. Sabatier, J. B. Senderens, *C. R. Acad. Sci.* **1902**, 134, 689–691.
- [9] P. Sabatier, J. B. Senderens, *C. R. Acad. Sci.* **1902**, 134, 514–516.
- [10] G. A. Mills, F. W. Steffgen, *Catal. Rev.* **1974**, 8 (1), 159–210. DOI: <https://doi.org/10.1080/01614947408071860>
- [11] E. Baraj, S. Vagaský, T. Hlinčík, K. Ciahotný, V. Tekáč, *Chem. Pap.* **2016**, 70 (4), 395–403. DOI: <https://doi.org/10.1515/chempap-2015-0216>
- [12] K. P. Brooks, J. Hu, H. Zhu, R. J. Kee, *Chem. Eng. Sci.* **2007**, 62 (4), 1161–1170. DOI: <https://doi.org/10.1016/j.ces.2006.11.020>
- [13] W. Wei, G. Jinlong, *Front. Chem. Sci. Eng.* **2011**, 5 (1), 2–10. DOI: <https://doi.org/10.1007/s11705-010-0528-3>
- [14] C. I. Melo, D. Rente, M. Da Nunes Ponte, E. Bogel-Lukasik, L. C. Branco, *ACS Sustainable Chem. Eng.*, in press. DOI: <https://doi.org/10.1021/acssuschemeng.8b06877>
- [15] K. Stangeland, D. Kalai, H. Li, Z. Yu, *Energy Procedia* **2017**, 105, 2022–2027. DOI: <https://doi.org/10.1016/j.egypro.2017.03.577>
- [16] W. A. Wan Abu Bakar, R. Ali, N. S. Mohammad, *Arabian J. Chem.* **2015**, 8 (5), 632–643. DOI: <https://doi.org/10.1016/j.arabjc.2013.06.009>
- [17] X. Su, J. Xu, B. Liang, H. Duan, B. Hou, Y. Huang, *J. Energy Chem.* **2016**, 25 (4), 553–565. DOI: <https://doi.org/10.1016/j.jechem.2016.03.009>
- [18] B. Miao, S. S. K. Ma, X. Wang, H. Su, S. H. Chan, *Catal. Sci. Technol.* **2016**, 6 (12), 4048–4058. DOI: <https://doi.org/10.1039/C6CY00478D>
- [19] A. Borgschulte, N. Gallandat, B. Probst, R. Suter, E. Callini, D. Ferri, Y. Arroyo, R. Erni, H. Geerlings, A. Züttel, *Phys. Chem. Chem. Phys.* **2013**, 15 (24), 9620–9625. DOI: <https://doi.org/10.1039/c3cp51408k>
- [20] P. Frontera, A. Macario, M. Ferraro, P. Antonucci, *Catalysts* **2017**, 7 (12), 59. DOI: <https://doi.org/10.3390/catal7020059>
- [21] S. J. Choe, H. J. Kang, S. J. Kim, S. B. Park, D. H. Park, D. S. Huh, *Bull. Korean Chem. Soc.* **2005**, 26 (11), 1682–1688. DOI: <https://doi.org/10.5012/bkcs.2005.26.11.1682>
- [22] G. D. Weatherbee, C. H. Bartholomew, *J. Catal.* **1982**, 77 (2), 460–472. DOI: [https://doi.org/10.1016/0021-9517\(82\)90186-5](https://doi.org/10.1016/0021-9517(82)90186-5)
- [23] J. Coenen, P. van Nisselrooy, M. de Croon, P. van Dooren, R. van Meerten, *Appl. Catal.* **1986**, 25 (1–2), 1–8. DOI: [https://doi.org/10.1016/s0166-9834\(00\)81215-4](https://doi.org/10.1016/s0166-9834(00)81215-4)
- [24] M. Frey, D. Édouard, A.-C. Roger, *C. R. Chim.* **2015**, 18 (3), 283–292. DOI: <https://doi.org/10.1016/j.crci.2015.01.002>
- [25] *Das Power-to-Methane-Konzept* (Eds: K. Ghaib), Springer, Wiesbaden **2017**.
- [26] J. Kirchner, J. K. Anollec, H. Lösch, S. Kureti, *Appl. Catal., B* **2018**, 223, 47–59. DOI: <https://doi.org/10.1016/j.apcatb.2017.06.025>
- [27] M.-A. Serrer, A. Gaur, J. Jelic, S. Weber, C. Fritsch, A. H. Clark, E. Saraçi, F. Studt, J.-D. Grunwaldt, *Catal. Sci. Technol.* **2020**, 10 (22), 7542–7554. DOI: <https://doi.org/10.1039/D0CY01396J>
- [28] T. Franken, A. Heel, *J. CO<sub>2</sub> Util.* **2020**, 39, 101175. DOI: <https://doi.org/10.1016/j.jcou.2020.101175>
- [29] J. Sehested, K. E. Larsen, A. L. Kustov, A. M. Frey, T. Johannessen, T. Bligaard, M. P. Andersson, J. K. Nørskov, C. H. Christensen, *Top. Catal.* **2007**, 45 (1–4), 9–13. DOI: <https://doi.org/10.1007/s11244-007-0232-9>
- [30] M. Guo, G. Lu, *React. Kinet., Mech. Catal.* **2014**, 113 (1), 101–113. DOI: <https://doi.org/10.1007/s11144-014-0732-0>
- [31] Y. R. Dias, O. W. Perez-Lopez, *J. Environ. Chem. Eng.* **2021**, 9 (1), 104629. DOI: <https://doi.org/10.1016/j.jece.2020.104629>
- [32] X. Li, Y. Wang, G. Zhang, W. Sun, Y. Bai, L. Zheng, X. Han, Le Wu, *ChemistrySelect* **2019**, 4 (3), 838–845. DOI: <https://doi.org/10.1002/slct.201803369>
- [33] Z. Li, T. Zhao, L. Zhang, *Appl. Organomet. Chem.* **2018**, 32 (5), e4328. DOI: <https://doi.org/10.1002/aoc.4328>
- [34] M. A. Paviotti, B. M. Faroldi, L. M. Cornaglia, *J. Environ. Chem. Eng.* **2021**, 9 (3), 105173. DOI: <https://doi.org/10.1016/j.jece.2021.105173>
- [35] L. Wei, H. Grénman, W. Haije, N. Kumar, A. Aho, K. Eränen, L. Wei, W. de Jong, *Appl. Catal., A* **2021**, 612, 118012. DOI: <https://doi.org/10.1016/j.apcata.2021.118012>
- [36] Y. Ma, J. Liu, M. Chu, J. Yue, Y. Cui, G. Xu, *Catal. Lett.* **2020**, 150 (5), 1418–1426. DOI: <https://doi.org/10.1007/s10562-019-03033-w>
- [37] W. Gac, W. Zawadzki, M. Rotko, G. Slowik, M. Greluk, *Top. Catal.* **2019**, 62 (5–6), 524–534. DOI: <https://doi.org/10.1007/s11244-019-01148-3>
- [38] Z. Li, B. Li, Z. Li, X. Rong, *Kinet. Catal.* **2015**, 56 (3), 329–334. DOI: <https://doi.org/10.1134/S0023158415030143>
- [39] K. Zhao, Z. Li, L. Bian, *Front. Chem. Sci. Eng.* **2016**, 10 (2), 273–280. DOI: <https://doi.org/10.1007/s11705-016-1563-5>
- [40] T. an Le, J. K. Kang, E. D. Park, *Top. Catal.* **2018**, 61 (15–17), 1537–1544. DOI: <https://doi.org/10.1007/s11244-018-0965-7>
- [41] Z. Li, L. Zhang, K. Zhao, L. Bian, *Trans. Tianjin Univ.* **2018**, 24 (5), 471–479. DOI: <https://doi.org/10.1007/s12209-018-0126-x>
- [42] S. Abate, C. Mebrahtu, E. Giglio, F. Deorsola, S. Bensaid, S. Perathoner, R. Pirone, G. Centi, *Ind. Eng. Chem. Res.* **2016**, 55 (16), 4451–4460. DOI: <https://doi.org/10.1021/acs.iecr.6b00134>
- [43] X. Bai, S. Wang, T. Sun, *React. Kinet., Mech. Catal.* **2014**, 112 (2), 437–451. DOI: <https://doi.org/10.1007/s11144-014-0700-8>

- [44] J. Moulijn, A. van Diepen, F. Kapteijn, *Appl. Catal., A* **2001**, 212 (1–2), 3–16. DOI: [https://doi.org/10.1016/S0926-860X\(00\)00842-5](https://doi.org/10.1016/S0926-860X(00)00842-5)
- [45] <https://gestis.dguv.de/data?name=008230> (Accessed on April 20, 2021)
- [46] S. H. Ewald, *Investigation of the Deactivation Behavior of Ni-Al Catalysts for CO<sub>2</sub> Methanation*, Dissertation, TU München **2019**.
- [47] <https://gestis.dguv.de/data?name=001280> (Accessed on April 20, 2021)
- [48] <https://gestis.dguv.de/data?name=109356> (Accessed on April 20, 2021)
- [49] <https://gestis.dguv.de/data?name=001780> (Accessed on April 20, 2021)
- [50] J. R. Rostrup-Nielsen, K. Pedersen, J. Sehested, *Appl. Catal., A* **2007**, 330, 134–138. DOI: <https://doi.org/10.1016/j.apcata.2007.07.015>
- [51] G. A. Fuentes, *Appl. Catal.* **1985**, 15 (1), 33–40. DOI: [https://doi.org/10.1016/S0166-9834\(00\)81484-0](https://doi.org/10.1016/S0166-9834(00)81484-0)
- [52] C. H. Bartholomew, *Appl. Catal., A* **2001**, 212 (1–2), 17–60. DOI: [https://doi.org/10.1016/S0926-860X\(00\)00843-7](https://doi.org/10.1016/S0926-860X(00)00843-7)
- [53] S. Ewald, M. Kolbeck, T. Kratky, M. Wolf, O. Hinrichsen, *Appl. Catal., A* **2019**, 570, 376–386. DOI: <https://doi.org/10.1016/j.apcata.2018.10.033>
- [54] E. Ruckenstein, B. Pulvermacher, *AIChE J.* **1973**, 19 (2), 356–364. DOI: <https://doi.org/10.1002/aic.690190222>
- [55] J. Sehested, *J. Catal.* **2004**, 223 (2), 432–443. DOI: <https://doi.org/10.1016/j.jcat.2004.01.026>
- [56] J. Sehested, J. A. Gelten, S. Helveg, *Appl. Catal., A* **2006**, 309 (2), 237–246. DOI: <https://doi.org/10.1016/j.apcata.2006.05.017>
- [57] I. Champon, A. Bengaouer, A. Chaise, S. Thomas, A.-C. Roger, *Catalysts* **2020**, 10 (12), 1477. DOI: <https://doi.org/10.3390/catal10121477>
- [58] I. Champon, A. Bengaouer, A. Chaise, S. Thomas, A.-C. Roger, *J. CO<sub>2</sub> Util.* **2019**, 34, 256–265. DOI: <https://doi.org/10.1016/j.jcou.2019.05.030>
- [59] M. Argyle, C. H. Bartholomew, *Catalysts* **2015**, 5 (1), 145–269. DOI: <https://doi.org/10.3390/catal5010145>
- [60] C. H. Bartholomew, J. B. Butt, *Catalyst Deactivation, 1991*, Studies in Surface Science and Catalysis, Vol. 68, Elsevier, Amsterdam **1991**.
- [61] J. Zhang, Z. Xin, X. Meng, M. Tao, *Fuel* **2013**, 109, 693–701. DOI: <https://doi.org/10.1016/j.fuel.2013.03.037>
- [62] M.-T. Fan, K.-P. Miao, J.-D. Lin, H.-B. Zhang, D.-W. Liao, *Appl. Surf. Sci.* **2014**, 307, 682–688. DOI: <https://doi.org/10.1016/j.apsusc.2014.04.098>
- [63] S. Wang, Z. Tian, Q. Liu, Y. Qiao, Y. Tian, *Main Group Met. Chem.* **2018**, 41 (3–4), 73–89. DOI: <https://doi.org/10.1515/mgmc-2018-0003>
- [64] J. W. Han, C. Kim, J. S. Park, H. Lee, *ChemSusChem* **2014**, 7 (2), 451–456. DOI: <https://doi.org/10.1002/cssc.201301134>
- [65] D. Türks, H. Mena, U. Armbruster, A. Martin, *Catalysts* **2017**, 7 (5), 152. DOI: <https://doi.org/10.3390/catal7050152>
- [66] S. Pérez, J. J. Aragón, I. Peciña, E. J. Garcia-Suarez, *Top. Catal.* **2019**, 62 (5–6), 518–523. DOI: <https://doi.org/10.1007/s11244-019-01139-4>
- [67] B. Legras, V. V. Ordonsky, C. Dujardin, M. Virginie, A. Y. Khodakov, *ACS Catal.* **2014**, 4 (8), 2785–2791. DOI: <https://doi.org/10.1021/cs500436f>
- [68] D. Liu, B. Li, J. Wu, Y. Liu, *Environ. Chem. Lett.* **2020**, 18 (1), 113–128. DOI: <https://doi.org/10.1007/s10311-019-00925-6>
- [69] S. Appari, V. M. Janardhanan, R. Bauri, S. Jayanti, *Int. J. Hydrogen Energy* **2014**, 39 (1), 297–304. DOI: <https://doi.org/10.1016/j.ijhydene.2013.10.056>
- [70] P. Kripylo, J. Hamann, M. Dinse, E. Ahmed, R. Mabroka, *J. Prakt. Chem.* **1992**, 334, 105–113.
- [71] C. Vogt, E. Groeneveld, G. Kamsma, M. Nachtegaal, L. Lu, C. J. Kiely, P. H. Berben, F. Meirer, B. M. Weckhuysen, *Nat. Catal.* **2018**, 1 (2), 127–134. DOI: <https://doi.org/10.1038/s41929-017-0016-y>
- [72] J. R. Rostrup-Nielsen, *J. Catal.* **1968**, 11 (3), 220–227. DOI: [https://doi.org/10.1016/0021-9517\(68\)90035-3](https://doi.org/10.1016/0021-9517(68)90035-3)
- [73] J. L. Oliphant, R. W. Fowler, R. B. Pannell, C. H. Bartholomew, *J. Catal.* **1978**, 51 (2), 229–242. DOI: [https://doi.org/10.1016/0021-9517\(78\)90297-X](https://doi.org/10.1016/0021-9517(78)90297-X)
- [74] D. Méndez-Mateos, V. L. Barrio, J. M. Requies, J. F. Cambra, *RSC Adv.* **2020**, 10 (28), 16551–16564. DOI: <https://doi.org/10.1039/D0RA00882F>
- [75] C. H. Bartholomew, *Catal. Rev.* **1982**, 24 (1), 67–112. DOI: <https://doi.org/10.1080/03602458208079650>
- [76] D. L. Trimm, *Catal. Rev.* **1977**, 16 (1), 155–189. DOI: <https://doi.org/10.1080/03602457708079636>
- [77] H. J. G. McCarty, *J. Catal.* **1979**, 57 (3), 406–416. DOI: [https://doi.org/10.1016/0021-9517\(79\)90007-1](https://doi.org/10.1016/0021-9517(79)90007-1)
- [78] J. Gao, Y. Wang, Y. Ping, D. Hu, G. Xu, F. Gu, F. Su, *RSC Adv.* **2012**, 2 (6), 2358. DOI: <https://doi.org/10.1039/c2ra00632d>
- [79] D. C. Gardner, C. H. Bartholomew, *Ind. Eng. Chem. Prod. Res. Dev.* **1981**, 20 (1), 80–87.
- [80] C. Mebrahtu, S. Perathoner, G. Giorgianni, S. Chen, G. Centi, F. Krebs, R. Palkovits, S. Abate, *Catal. Sci. Technol.* **2019**, 9 (15), 4023–4035. DOI: <https://doi.org/10.1039/C9CY00744J>
- [81] N. Elia, J. Estephane, C. Poupin, B. El Khoury, L. Pirault-Roy, S. Aouad, E. A. Aad, *ChemCatChem* **2021**, 13 (6), 1559–1567. DOI: <https://doi.org/10.1002/cctc.202001687>
- [82] X. Guo, Z. Peng, M. Hu, C. Zuo, A. Traitangwong, V. Meeyoo, C. Li, S. Zhang, *Ind. Eng. Chem. Res.* **2018**, 57 (28), 9102–9111. DOI: <https://doi.org/10.1021/acs.iecr.8b01619>
- [83] B. Mutz, P. Sprenger, W. Wang, Di Wang, W. Kleist, J.-D. Grunwaldt, *Appl. Catal., A* **2018**, 556, 160–171. DOI: <https://doi.org/10.1016/j.apcata.2018.01.026>
- [84] S. Theurich, S. Rönsch, R. Güttel, *Energy Technol.* **2020**, 8 (3), 1901116. DOI: <https://doi.org/10.1002/ente.201901116>
- [85] B. Kreitz, J. Friedland, R. Güttel, G. D. Wehinger, T. Turek, *Chem. Ing. Tech.* **2019**, 91 (5), 576–582. DOI: <https://doi.org/10.1002/cite.201800191>
- [86] B. Mutz, H. W. P. Carvalho, W. Kleist, J.-D. Grunwaldt, *J. Phys.: Conf. Ser.* **2016**, 712, 12050. DOI: <https://doi.org/10.1088/1742-6596/712/1/012050>
- [87] B. Mutz, A. Gänzler, M. Nachtegaal, O. Müller, R. Frahm, W. Kleist, J.-D. Grunwaldt, *Catalysts* **2017**, 7 (9), 279. DOI: <https://doi.org/10.3390/catal7090279>
- [88] J. Bremer, K. H. G. Rätzke, K. Sundmacher, *AIChE J.* **2017**, 63 (1), 23–31. DOI: <https://doi.org/10.1002/aic.15496>
- [89] A. Fache, F. Marias, V. Guerré, S. Palmade, *Waste Biomass Valorization* **2020**, 11 (2), 447–463. DOI: <https://doi.org/10.1007/s12649-018-0507-3>
- [90] S. Rönsch, A. Ortwein, S. Dietrich, *Chem. Eng. Technol.* **2017**, 40 (12), 2314–2321. DOI: <https://doi.org/10.1002/ceat.201700229>
- [91] S. Rönsch, S. Matthischke, M. Müller, P. Eichler, *Chem. Ing. Tech.* **2014**, 86 (8), 1198–1204. DOI: <https://doi.org/10.1002/cite.201300046>
- [92] S. Rönsch, J. Schneider, S. Matthischke, M. Schlüter, M. Götz, J. Lefebvre, P. Prabhakaran, S. Bajohr, *Fuel* **2016**, 166, 276–296. DOI: <https://doi.org/10.1016/j.fuel.2015.10.111>
- [93] L. L. P. Forzatti, *Catal. Today* **1999**, 52, 165–181.